

Re-Naturing Cities: Evaluating the effects on future air quality in the city of Porto

S. Rafael^{*}, B. Augusto, A. Ascenso, C. Borrego, A.I. Miranda

CESAM, Department of Environment and Planning, University of Aveiro, 3810-193, Aveiro, Portugal

HIGHLIGHTS

- Cities must become resilient to be able to deal with future air pollution.
- Different “green” measures were studied using the WRF-CHIMERE modelling setup.
- Green roofs, white roofs and white surfaces increases PM10 and NO₂ concentrations.
- Green urban areas decreases PM10 and NO₂ concentrations and increases O₃ levels.
- Double effects were found, showing the need of knowledge-based urban planning.

ARTICLE INFO

Keywords:

Air quality
Climate change
Nature-based solutions
Numerical models
Urban areas

ABSTRACT

The effect of different “green” measures, such as the increase of urban green areas, the application of green roofs and the increase of surfaces albedo on urban air quality were evaluated with the WRF-CHIMERE modelling system. In order to account for the heterogeneity of urban areas, a single layer urban canopy model was coupled to the WRF model. The case study consists of a heat wave occurring in the Porto (Portugal) urban area in a future climate scenario, considering the Representative Concentration Pathway RCP8.5. The influence of the selected measures on PM10, NO₂ and O₃ concentrations was quantified and compared with a control run (without measures) simulation scenario. The results revealed that all the measures are able to mitigate the effects of heat waves by reducing the air temperature between -0.5 °C and -1 °C (maximum differences for the mean of the episode). Positive and negative effects were found in terms of air quality. The implementation of green roofs and the increase of surfaces albedo promoted an overall increase of PM10 (between +0.6% and +1.5%) and NO₂ (between +0.8% and 3.5%) concentrations, which are closely related to a decrease of vertical mixing in the urban boundary layer. The increase of green urban areas promoted an overall decrease (on average) of both PM10 and NO₂, by around -1% and -3% , respectively. The O₃ levels increased with the increase of urban green areas, mostly located over the Porto urban area. Slight differences were promoted by the implementation of green roofs. For the increase of surfaces albedo, both increases and decreases of O₃ concentrations were observed. The obtained results contribute to the knowledge of the chemical composition of the urban atmosphere and can be of great importance for stakeholders and decision-makers to deal with climate change impacts.

1. Introduction

Cities only cover a small fraction of the Earth (approximately 2% of the land surface). Despite that, given the large and ever-increasing fraction of the world’s population living in cities, and the disproportionate share of resources used by these urban residents, cities and their inhabitants are key drivers of global environmental change. Urban areas are the major sources of greenhouse gases; while the exact number is

debated, overall 70%–90% of carbon emissions are generated in cities (EEA, 2017). These statistics reveal a straight linkage between cities and climate change. Cities are the main contributor to climate change; however, cities are highly vulnerable to climate change effects since extreme weather events can be especially disruptive to complex urban systems and due to the high level of urbanization and demographic growth.

Cities are a main source of air pollutants too and despite the different

^{*} Corresponding author.

E-mail address: sandra.rafael@ua.pt (S. Rafael).

<https://doi.org/10.1016/j.atmosenv.2019.117123>

Received 12 August 2019; Received in revised form 5 November 2019; Accepted 7 November 2019

Available online 8 November 2019

1352-2310/© 2019 Elsevier Ltd. All rights reserved.

processes involved in atmospheric pollution and climate change, they are linked in several key ways. In light of that, several air quality studies have been conducted under future climate based on numerical tools. Sá et al. (2016) classified these studies in three main categories, according to their characteristics: i) studies that only consider the effect of climate change, by keeping the anthropogenic emissions constant (e.g., Manders et al., 2012); ii) studies that maintain the meteorological conditions constant (same as the historical year) in future scenarios and only change the air pollutant emission inventories (e.g., Zhang et al., 2010); and iii) studies that consider future climate along with the modification of anthropogenic emissions (Markakis et al., 2014).

Notwithstanding the set of air quality studies performed under climate change conducted over the last years, the majority of these studies were focused on global or regional level, not reaching a higher detail (urban or city scale). Sá et al. (2016) evaluated air quality over mainland Portugal and over Porto urban area in 2050 under the RCP8.5 scenarios, using high spatial resolution modelling and emission scenarios at urban scale. Results showed an increase in the occurrence, duration and intensity of extreme values of PM10 and O₃, surpassing the annual legislated values and registering a higher number of daily exceedances. Considering the climate change effects alone, results showed an increase of the NO₂ and PM10 annual means in both Portugal and Porto urban area. Overall, an air quality degradation is expected over Portugal for the medium-term climate future (2046–2065), which implies warmer and dryer conditions and an increase of background concentrations of ozone and particulate matter. These results highlight the notion that climate change is a systemic challenge for cities. Despite of that, cities have a unique ability to address global climate change challenges, by applying local measures to deal with specific vulnerabilities and needs (EEA, 2016). Due to the European Research and Innovation policy agenda on Nature-Based Solutions and Re-Naturing Cities, a set of studies have been conducted to investigate the capability of these solution as adaptation measures. These solutions, also called green measures, provide sustainable, cost-effective, multi-purpose and flexible alternatives for various objectives (EC, 2015). Fallmann et al. (2016) investigated the effect of different urban heat island (UHI) green mitigation measures on urban air quality, addressing carbon monoxide (CO), nitrogen monoxide (NO) and ozone (O₃) air pollutants. The study was focused on a heat wave period of 2003 for the urban area of Stuttgart. Epstein et al. (2017) evaluated the air quality effects of cool-roofs, at nowadays meteorological conditions, on O₃ and particulate matter with an aerodynamic diameter equal or less than 2.5 µm (PM_{2.5}) concentrations. Chen et al. (2018) quantified the effects of urbanization on regional climate and air quality and the influence of UHI mitigation measures on urban air quality in Beijing, focusing on O₃ levels. Despite the features of each study, all of them concluded that the implementation of nature based solutions can promote both positive and negative benefits depending on the measure to be implemented and on the cities characteristics, e.g., its dimension, location, population density, and microclimate. Also, all the studies recognized that further works in this scientific field are needed. A complete literature review of the way of how green measures has been addressed in microscale and macroscale air pollution dispersion models can be found in Tiwari et al. (2019).

The main goal of this study is to investigate and quantify the effectiveness of different green measures in improving air quality under a future heat wave (medium-term future climate), at Porto urban area. Three main urban air pollutants were analysed: particulate matter with an aerodynamic diameter equal or less than 10 µm (PM₁₀), nitrogen dioxide (NO₂) and O₃. This work is distinguishable from previous ones in three main aspects: i) the majority of the studies has been conducted to assess the capability of green measures to mitigate high urban temperatures or urban heat island effects, without a focus on air quality; ii) the majority of the studies that address air quality only analyse the impacts of vegetation across roadsides in restricted study domains (microscale studies); the works performed at a regional scale are mainly conducted

for present meteorological conditions and only analyse one of the three identified air pollutants; iii) few studies were conducted using future climate projections and downscaled to regional areas with high level of spatial resolution. Moreover, such study was never performed for the Porto urban area, one of the urban areas most exposed to heat waves exacerbation due to climate changes (Lau et al., 2015), nor to any Portuguese city or urban environment.

The paper is structured as follows: section 2 describes the case study and the modelling setup methodology, including a brief description of the applied models and their configuration for the simulations. A description of the “green” measures under study is also presented in section 2. The implications of the “green” measures on the meteorological variables and on the air quality of the study area is analysed and discussed in section 3. Conclusions follow in section 4.

2. Data and methods

A specific methodology was applied to assess the influence of the application of “green” measures in the air quality of Porto Urban Area. Two main steps were performed: i) definition of a modelling setup (section 2.2); and ii) selection of green measures (section 2.3). A detailed description is presented in the following sub-sections.

2.1. Case study

Porto urban area is located in the northwest of Portugal and is one of the largest and most densely populated urban area in the country (represents almost 25% of Portugal’s urban land use), with near 1.8 million inhabitants (INE, 2011). It was identified as one of the European cities where the urban fringe has grown faster (EEA, 2011), resulting in a depletion of agricultural land and forests. As result of the high rate of urbanization, Porto stands out as the Portuguese urban area with the least share of green and blue areas (Amorim et al., 2013).

Porto’s climate is relatively mild (in summer temperatures varies between 15 and 25 °C range and in winter between 5 and 15 °C); however, it shows a high temperature and precipitation seasonality and inter-annual variability. The projected future climate trends for the Porto urban area indicates an average increase of almost 2 °C in the medium-term future (2046–2065), which can almost double by the end of the current century (3.7 °C), with an increase of the annual number of consecutive dry days (Borrego et al., 2015; Marta-Almeida et al., 2016). It is expected that the occurrence of heat waves in this area, which is not a major concern nowadays, can double (around 2.2 times more than in the recent past) by the medium-term future and increase by a factor of 3.6 in the long-term future, particularly for the summer periods (Carvalho et al., 2017). The effects of these changing of climate conditions on people will be aggravated by the poor building insulation, leading to increased probability of severe human health consequences when extreme events such as heat waves occur (Monteiro and Velho, 2014).

The work of Carvalho et al. (2017) has used high-resolution climatic dataset to identify the occurrence of heat waves in Porto urban area in a medium-term future period (2046–2065). This selection was made following the methodology described in Russo et al. (2014). In short, this methodology defines as a heat wave at least three consecutive days with daily maximum temperature above a daily threshold (90th percentile of daily maxima centred on a 31 day window) (Carvalho et al., 2014; Fonseca et al., 2016). Five heat waves were identified following this approach and considered as “heat wave episodes”. The heat wave with highest extreme temperatures – 24th to 26th of July 2049 (temperatures above 35 °C during three consecutive days) – was selected as case study for the present work.

Due to its dimension and economic importance, Porto urban area has been facing air quality problems. The air quality status of the study area was investigated by analysing the measured data acquired over a 5-years period (2013–2017). Air quality monitoring stations located in the study region and classified as urban were used to assess the PM₁₀, NO₂ and O₃

trend lines. A total of six air quality stations were used (three classified as urban traffic and three classified as urban background). The urban background stations showed a concentration reduction trend for PM₁₀ and O₃ through the years. The annual PM₁₀ concentration in 2017 was 19.6% (average of two stations) less than the value registered in 2013, while for O₃, the annual concentration in 2017 was 26.9% (average of three stations) less than the value registered in 2013 (average of three stations) (see Table S1 in the Supporting Information). Negative (decrease of concentrations) and positive (increase of concentrations) trends were observed for NO₂ concentrations. All stations showed a tendency to reduce NO₂ concentrations; however, an increase of concentrations was observed in 2016 (+26.9%) and 2017 (+18.7%) in one urban background station, compared with the levels registered in 2013. No exceedances to the annual limit value of PM₁₀ and NO₂ concentrations were observed. For the analysed period, exceedances to the NO₂ hourly limit value were obtained in less than 1% of the times, while exceedances to the PM₁₀ daily limit value varied between 1% and 4% of the times (depending of the air quality station). The O₃ information threshold was exceeded 6 times maximum in the last 5-years.

Similar trends were observed at the urban traffic stations (see Table S2 in the Supporting Information), namely a systematic decrease of annual PM₁₀ concentrations through the years in all stations. The tendency of reduction of the annual NO₂ concentrations has been changing in last years. In 2017, an increase of +45.4% (54.3 $\mu\text{g m}^{-3}$) and +17.5% (30.8 $\mu\text{g m}^{-3}$), compared to the levels registered in 2013, was observed in two of the three stations analysed. The PM₁₀ annual average was exceeded in 2016, while the NO₂ annual average was exceeded between 2014 and 2017 at one urban traffic station.

Highest PM₁₀ concentrations were always registered in the winter months (November–February) (Fig. S1 and Fig. S2 in the Supporting Information). Since no noteworthy changes occur in the road traffic volume in these months (compared with the entire year), these data highlight the influence of non-road emission sources on the air quality of the study area, in particular residential combustion. High PM₁₀ concentrations are also obtained, in some years, in summer months (August–September), due to dust episodes. These results are aligned with the conclusions made by Gama et al. (2018). The NO₂ concentrations follow the traffic dynamic and the traffic-related NO_x emissions, as occurs in the majority of the European urban areas (Vicente et al., 2018).

The expected changes in the climate and the air quality trends, associated with the fact that citizens and the urban morphology are not yet prepared to deal with these issues, make this city an interesting and challenging case study to evaluate the potentialities of a “green” strategy.

2.2. Modelling setup

A modelling system composed by the WRF-CHIMERE models was applied to the study period (24th to 26th of July 2049). The Weather Research and Forecasting (WRF) model (Skamarock et al., 2008), version 3.7, coupled with the single layer urban canopy model (SLUCM) (Kusaka et al., 2001; Kusaka and Kimura, 2004), was used. This cross-scale atmospheric modelling system provides a prediction of meteorological conditions from regional scale to microscale. Thus it has been widely applied to address future climate change impacts in urban environments supporting the development of mitigation and adaptation strategies to deal with the extreme meteorological events (Chen et al., 2011). The SLUCM is available as a WRF model module, which coupling is made through the Noah land surface model (LSM). The SLUCM takes into account the impacts of urban areas morphology on the surface-atmosphere exchanges; this means that for a given grid cell the LSM calculates the surface fluxes for natural areas (trees, parks, etc.) whereas the SLUCM provides the surface fluxes for the artificial surface (Chen et al., 2011). A detailed description of the WRF urban modelling system can be found in Chen et al. (2011).

The WRF-SLUCM was set up with four domains (see Fig. 1). The

outer domain (D1), covers Europe and North of Africa and has 173×142 horizontal grid cells with horizontal resolution of 27 km; the nested domain D2 covers the Iberian Peninsula and has 75×166 horizontal grid cells with a horizontal resolution of 9 km; D3 covers the Northwest of Portugal and has 121×109 horizontal grid cells with a horizontal resolution of 3 km; and D4 covers the Porto urban area and has 34×34 horizontal grid cells with horizontal resolution of 1 km. The vertical grid was composed by 30 vertical layers up to the top of the computational domain (50 hPa). The two-way nesting technique was applied for the simulations (Skamarock et al., 2008). The Dudhia shortwave radiation scheme (Dudhia, 1989) and the RRTM (Rapid Radiative Transfer Model) longwave radiation scheme (Mlawer et al., 1997) were also used. The Yonsei University (YSU) scheme (Hong et al., 2006) was used to calculate the vertical turbulent mixing of momentum and scalars. The YSU scheme has been widely applied to meteorological and environmental modelling due to its performance in a well-mixed atmospheric boundary layer and computational efficiency (Marta-Almeida et al., 2016). Grid-scale clouds were resolved using the WRF single moment 5-class scheme (Hong and Lim, 2006), while subgrid-scale convective clouds (cumulus parameterization scheme) for lower resolution domains (D1, D2 and D3) were parameterized by the new Grell scheme (Grell, 1993; Grell and Devenyi, 2002).

The meteorological initial and boundary conditions were obtained from the Max Planck Institute Earth System Model – Lower Resolution (MPI-ESM-LR) (Giorgetta et al., 2013), with a horizontal resolution of 1.9° and with a temporal resolution of 6-h intervals. The MPI-ESM-LR global climate model was chosen since it is considered one of the best models to simulate the climate of Europe (Brands et al., 2013). The Representative Concentration Pathway Scenario RCP8.5 was adopted (Riahi et al., 2007) because it corresponds to the pathway with the highest greenhouse gas emissions, leading to a radiative forcing of 8.5 W m^{-2} at the end of the century (2100) (IPCC, 2013); therefore, it is the scenario that reflects more onerous impacts (Rafael et al., 2017).

Information regarding the land use/land cover was taken through a combination between the Corine land cover project (Büttner et al., 2006) 2006 version (CLC2006), with a 3 arc-seconds horizontal resolution, and the Porto Urban Atlas from the European Environmental Agency, with 10 m \times 10 m horizontal resolution, in a complementary approach to better detail Porto urban features. The Porto Urban Atlas was used for the domain areas covered by this database, while CLC2006 was used for areas where such data was not available. Both land use databases were remapped to the United States Geological Survey (USGS) 33 land use categories; the CLC2006 was remapped following the methodology proposed by Pineda et al. (2004), while the conversion of Porto Urban Atlas followed the methodology proposed by Carvalho et al. (2017). The USGS 33 land use categories considers 3 different urban categories: High Intensity Residential (land code 32), which includes highly developed areas where people reside in great number (apartment complexes, row houses, etc.); Low Intensity Residential (land code 31), which includes areas with a mixture of constructed materials and vegetation where population densities are lower than in high intensity residential areas (single-family housing units, etc); and Industrial/Commercial (land code 33), which includes infrastructures (roads, railroads, airports, harbours, etc.) and all other built areas that do not fit into residential categories. The urban categories cover 26.3% of the study domain, with the majority of these areas classified as Low Intensity Residential (19.1%). The remaining areas are classified as water bodies (29.2%) and as agriculture/forest areas (44.5%).

In order to better represent the sub-grid scale variability in land use/land cover composition, the Noah LSM was used with the sub-tiling option (described by Li et al., 2013). The SLUCM options to consider urban morphology (mean building and trees heights, and roof and road widths, building), urban irrigation, anthropogenic heating and evaporation over impervious surface were activated. The best set of urban parametrizations, found by Rafael et al. (2019) for the study area, were applied in this work. Despite the availability of other urban canopy

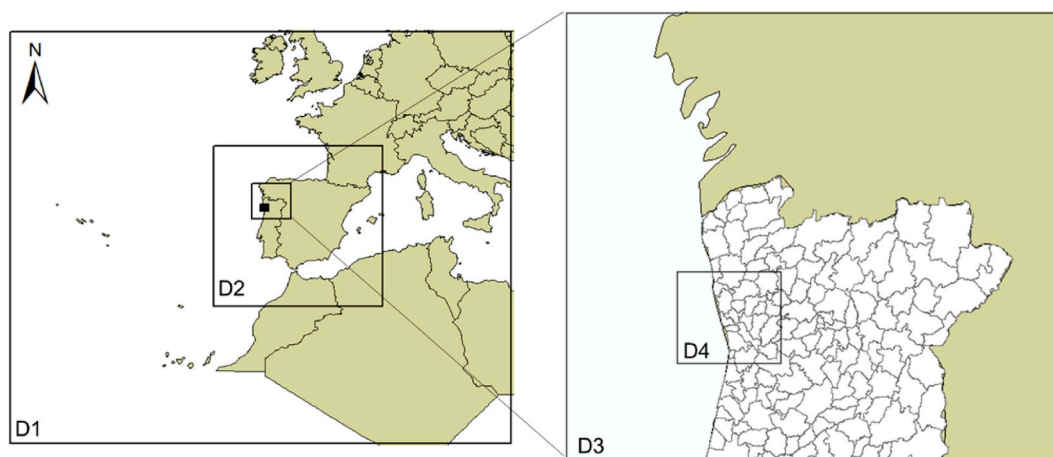


Fig. 1. Modelling-setup domains, D1: Europe and part of the North of Africa; D2: Iberian Peninsula; D3: North-western region of Portugal; D4: Porto urban area (study area, including 17 municipalities).

schemes in the WRF model (see [Fallmann et al., 2013](#)), the SLUCM was chosen since previous works, conducted to the study area, have shown that this model is suitable to simulate urban turbulence ([Carvalho et al., 2017](#); [Rafael et al., 2018, 2019](#)). [Table 1](#) summarizes the physical parameters used for the three urban classes. A detailed description of these options can be found in [Rafael et al. \(2019\)](#).

The CHIMERE chemistry-transport model is an open access multi-scale Eulerian chemical transport model (CTM), which applies the integration of the mass continuity equation to estimate the concentrations of several chemical species in each cell of a given grid. It was developed to simulate gas-phase chemistry ([Schmidt et al., 2001](#)), aerosol formation, transport and deposition ([Bessagnet et al., 2004](#);

[Vautard et al., 2005](#)) from regional to urban scales. As input data, the CHIMERE model requires meteorology, initial and boundary conditions, atmospheric emissions, land use and topography data.

CHIMERE v2016a1 was applied directly to the WRF grid, thus the domains and spatial resolution were the same as described in [Fig. 1](#). The LMDz-INCA (gas species and non-dust aerosols) ([Hauglustaine et al., 2004](#)) global chemical-transport model outputs were used to provide the initial and boundary conditions for the outermost domain. The anthropogenic emissions for the year 2015 were obtained from the European Monitoring and Evaluation Programme (EMEP) inventory ([Vestreng et al., 2004](#)). The biogenic emissions were calculated using the Model of Emissions of Gases and Aerosols from Nature (MEGAN) ([Guenther et al., 2006](#)), part of the CHIMERE model. The land use data came from the “United States Geological Survey” (USGS). As chemical mechanism, the model used MELCHIOR-2 to simulate the concentration of 44 gaseous species from a set of 120 chemical reactions. More detail on these parameterizations can be found in [Monteiro et al. \(2005\)](#). Regarding the vertical resolution, eight vertical layers were used with different thicknesses, the first layer had 20 m and the last extends to 500 hPa.

The full modelling setup is summarized in [Table 2](#).

The modelling setup was applied for the selected heat wave episode for the control run (considering the current urban morphology) and for “green” scenarios. The only difference between the control run and the scenarios was the inclusion of designed “green” solutions.

2.3. “Green” scenarios

The measures applied in this study were selected after a comprehensive literature review. The analysis was focused on studies discussing the advantages of different solutions to support cities to deal with the anticipated effects of climate change and extreme events and based on the objectives of the European strategy to Nature-Based Solutions and Re-Naturing Cities. The main criteria underlying this selection was the consistently reported effectiveness and benefits of the measures in the mitigation of heat waves effects in built-up surfaces.

From this analysis, four measures were selected: i) the introduction of green roofs in areas classified as built-up area; ii) the introduction of “cold” roofs in areas classified as built-up area; iii) the application of “light” surfaces in areas classified as built-up area; and iv) the duplication of existing green areas. Four different “green” scenarios were built using the selected measures.

Scenario 1 (S1) considers that 100% of the urban areas (i.e. the simulation grid cells with USGS land use urban categories as 31, 32 and 33) have green roofs (covered with vegetated surfaces). The green roof system, when compared to the conventional roof, adds three layers;

Table 1

Urban canopy parameters used for the three-urban land-use categories: low-intensity residential, high-intensity residential and commercial/industrial area.

Parameter	Unit	Specific Values for		
		Low-intensity residential	High-intensity residential	Commercial/industrial
Artificial surface fraction (F_{urb})	Fraction	0.2	0.8	0.7
Natural surface fraction (F_N)	Fraction	0.8	0.2	0.3
Mean building height	m	4	12	6
Mean trees height	m	4	4	4
Roof width	m	6	8	10
Road width	m	6.0	8.75	10.0
Anthropogenic heat flux	$W m^{-2}$	15	50	90
Heat capacity of roof and wall	$MJ m^{-3} K^{-1}$	1.0	1.0	1.0
Heat capacity of road	$MJ m^{-3} K^{-1}$	1.4	1.4	1.4
Thermal conductivity of roof and wall	$W m^{-1} K^{-1}$	0.45	0.45	0.45
Thermal conductivity of road	$W m^{-1} K^{-1}$	0.45	0.45	0.45
Surface albedo of roof and wall	Fraction	0.15	0.15	0.15
Surface albedo of road	Fraction	0.09	0.09	0.09
Surface emissivity of roof and wall	–	0.90	0.90	0.90
Surface emissivity of road	–	0.95	0.95	0.95

Table 2
WRF-CHIMERE model configuration.

		WRF		CHIMERE	
Parameter	Specification	Parameter	Specification	Parameter	Specification
dx, dy	1 km	Meteorological BC	1.9° MPI-ESM-LR	Land surface model	USGS database
West-east [grid cells]	34	Urbanization scheme	SLUCM	Chemical option	MELCHIOR-2
South-north [grid cells]	34	Microphysics options	WSM 5-class scheme	Emission inventory	EMEP
Vertical spacing	30 vertical levels	Shortwave radiation	Dudhia scheme	Chemical boundary	LMDz-INCA
	Lowest level: 10-m				
Time frame	24-26 of July 2049	Longwave radiation	RRTM scheme	Biochemistry	MEGAN global data
-	-	Land surface model	Noah LSM	Dry deposition	Wesely Parametrization

vegetation, soil and growing media layer. This system is integrated in WRF-SLUCM and is detailed in Yang et al. (2015). Scenario 2 (S2) considers that 100% of the buildings have white roofs (roofs painted white or covered with white materials). For these grid cells, the roof surface albedo was defined as 80%, which according to Susca (2012), is the appropriate value for the albedo of a white-color newly painted roof. Scenario 3 (S3) considers that all built-up surfaces have an albedo of 80% (see S2). This value was defined for the surface albedo of roofs, facades and ground. The modification of albedo (S2 and S3), enhances the reflected solar radiation of the built-up area, changing the urban energy balance by modifying the exchanges of the total heat flux between the surface and the atmosphere (Rafael et al., 2016). Scenario 4 (S4) considered an increase of Porto green urban areas (parks). To do that, the number of grid points that originally were considered as “green urban area” in the control run was identified. The number of grid points with this classification was then doubled and the land use category was changed to the USGS land use category 3 “Irrigated Cropland and Pasture”, according to the methodology defined by Carvalho et al. (2017).

3. Results and discussion

The effects of the “green” measures (scenarios S1 to S5) on the air quality under a future heat wave in the Porto urban area are displayed and discussed in this section (section 3.2.). A simple meteorological analysis was also undertaken to determine how the meteorological variables evolved in the scenarios (section 3.1.).

3.1. Meteorological analysis

To fully understand the effects of the selected measures on air quality, their influence on meteorological variables was also investigated. The meteorological variables were selected based on their importance to human comfort and their recognized influence on air quality modelling. Variables such as, 2 m temperature (T2), 10 m wind velocity (U10), planetary boundary layer height (PBLH), downward shortwave radiation (SWDOWN) and sensible heat flux (HFX) were used for this analysis. The analysis consisted in three different approaches: i) estimation of the absolute values of each scenario and calculation of the average differences between each scenario and the control run, considering the mean of the modelling period and using a weighted average to consider the different classification types of built-up land use (Table 3); ii) hourly average differences between the scenarios and the control run for the region as a whole (obtained through the weighted average of the meteorological variables, based on the land use proportions that exist in the domain), to assess the average behaviour of the study area, giving an idea of how the selected measures influence the meteorology of this region (Fig. 2); and iii) mapping of the differences (average of the modelling period) between the “green” scenarios and the control run (Fig. 3), to understand the spatial variability of the meteorological variables.

Looking at the built-up areas of the domain (Table 3), in average, the temperature is reduced in a range of -0.3% and -1.5% for the S4 and S3 scenarios, respectively. The magnitude of this reduction increases as more pronounced is the level of urbanization, with the maximum differences being obtained in the land use classified as “High intensity residential area” (land code 32). All analysed scenarios showed a

Table 3

Effect of “green” scenarios on 2 m temperature (T2), 10 m wind velocity (U10), planetary boundary layer height (PBLH), downward shortwave radiation (SWDOWN) and sensible heat flux (HFX) in the cells classified as built-up areas^a. Values are presented for the mean of the modelling period.

Scenarios	Land Use	Meteorological parameters				
		T2 (°C)	U10 (m·s ⁻¹)	PBLH (m)	SWDOWN (W·m ⁻²)	HFX (W·m ⁻²)
Control run	31	28.5	7.9	710.1	283.2	-104.2
	32	29.3	1.3	614.0	291.6	81.5
	33	29.9	1.7	680.7	276.7	70.5
	$\Delta\%$	-0.6	0.0	-1.8	0.0	-28.4
S1	31	28.4	7.9	708.4	283.2	-111.9
	32	29.1	1.3	587.6	291.6	52.3
	33	29.7	1.7	671.9	276.7	41.0
	$\Delta\%$	-0.6	0.0	-1.8	0.0	-28.4
S2	31	28.3	7.9	715.9	283.2	-115.7
	32	29.0	1.3	574.6	291.8	29.2
	33	29.7	1.7	636.2	276.8	22.1
	$\Delta\%$	-0.8	0.0	-3.9	0.0	-47.9
S3	31	28.1	7.9	716.5	283.1	-122.5
	32	28.8	1.3	604.3	291.7	-8.4
	33	29.5	1.7	716.6	276.7	-14.4
	$\Delta\%$	-1.5	0.0	+1.6	0.0	-62.3
S4	31	28.4	2.6	570.3	295.4	-80.8
	32	29.4	1.4	655.7	282.3	77.9
	33	29.6	3.5	653.6	285.7	7.9
	$\Delta\%$	-0.3	-31.2	-6.3	+1.4	-23.5

^a Land use classification: 31 – Low intensity residential; 32 – High intensity residential; 33 – Industrial or commercial.

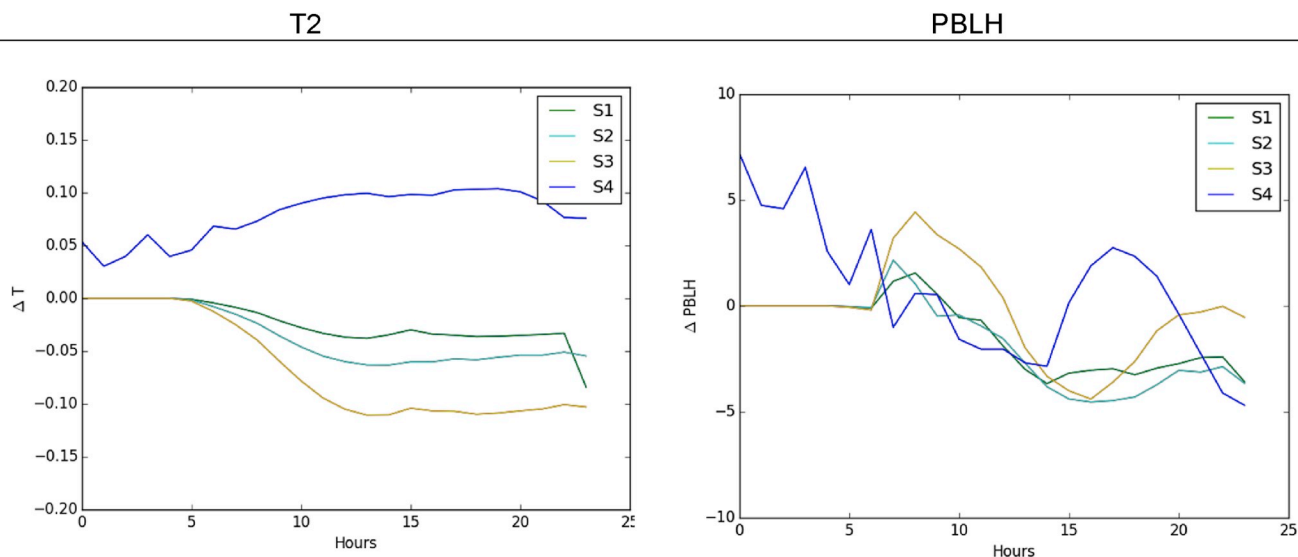


Fig. 2. Daily average differences (absolute values) of air temperature and boundary layer height for the selected heat-wave. S1: scenario considering the application of green roofs; S2: scenario considering the application of white roofs; S3: scenario considering white surfaces; S4: scenario considering the increase of parks. (For interpretation of the references to color in this figure legend, the reader is referred to the Web version of this article.)

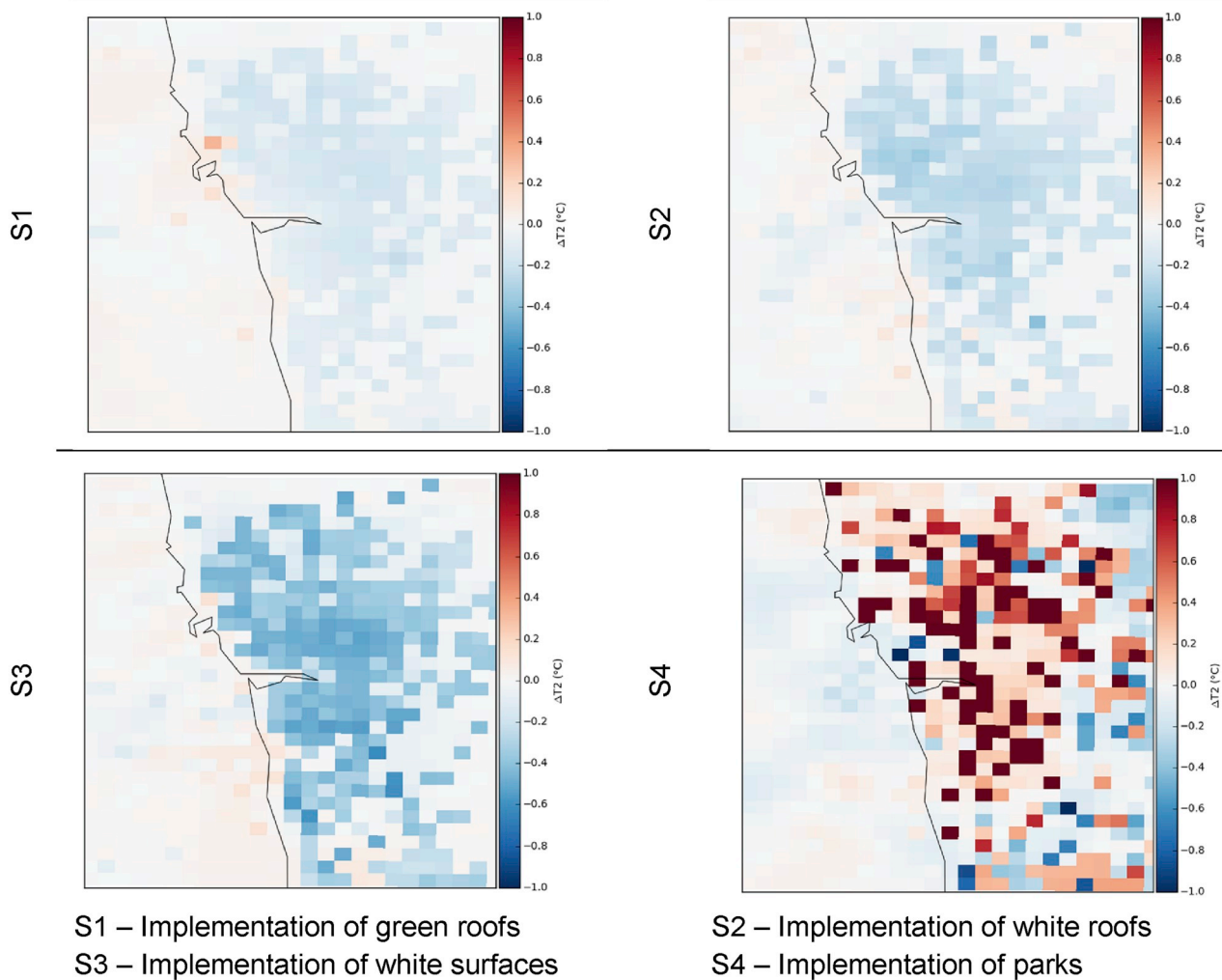


Fig. 3. Spatial distribution of the absolute differences between “green” scenarios and control run for temperature at 2 m. The differences are presented for the mean of the modelling period. (For interpretation of the references to color in this figure legend, the reader is referred to the Web version of this article.)

capability to decrease the near surface temperature locally. The temperature reduction related to the implementation of green roofs (S1 scenario) is justified by an increase of the surface moisture availability and to the evapotranspiration of the green vegetated surface (Carvalho et al., 2017). This increase has a direct impact on the atmosphere-surface exchanges, since an increase of the evapotranspiration process implies an increase of latent heat flux and, consequently, a decrease of sensible heat flux (Rafael et al., 2016). An average decrease in the sensible heat flux of -28.4% (varying between -7.4% and -41.8% for the land code 31 and 33, respectively) was obtained. This phenomenon is also seen in S4 (increasing of green urban areas), albeit in a less extent (-23.5% in average). Also, the vegetated areas have higher albedo when compared with built-up areas, which means that less amount of solar radiation is absorbed by the surface, keeping it cooler. For S4 scenario the shading effect over the ground plays an important role in the temperature reduction, by intercepting and absorbing solar radiation and reduction the amount of heat that reaches the surface (Rafael et al., 2016).

The implementation of white roofs (to increase the roof albedo) implies that a higher proportion of solar radiation is reflected by the surface and a higher amount of heat is dissipated. This means that less energy will be exchanged in the form of sensible heat flux (Rafael et al., 2016), promoting a temperature decrease. This effect is boosted in S3 scenario due to the higher extent of surfaces with an albedo of 80%, to mimic the application of white surfaces. An average reduction of the sensible heat flux of -15.3 W m^{-2} (S2 scenario) and -42.2 W m^{-2} (S3 scenario) was obtained; the higher reduction of sensible heat flux in S3 scenario is followed by a higher capability to reduce near surface temperature. Should be noted that, for S2 and S3 scenarios, the white roofs and facades properties (thermal and others) are the same as the conventional surfaces, with the exception of albedo.

The analysed scenarios showed no effect on the mean wind velocity, with the exception of S4 scenario. In this scenario, as a result of the land use changes (compared with the control run) two distinct behaviours were found: i) a decrease of wind velocity of almost -67% ; this change might be due to the fact that the lower near surface temperature leads to a loss of the buoyancy production term in the Turbulent Kinetic Energy (TKE) production equation, which results in a decrease of the friction velocity u^* (Fallmann et al., 2016); and ii) an increase of wind velocity of 1.8 m s^{-1} (in average) due to the decrease in roughness height by the replacement of buildings by vegetation. Slight changes were also found on the mean downward shortwave radiation in S4 scenario (an average increase of $+1.4\%$), related to the change of the net radiation promoted by a change of land use.

Changes in the planetary boundary layer height were found for all the analysed scenarios, with a general decrease ranging between -1.8% (12.3 m, S1 scenario) and -6.3% (41.7 m, S4 scenario), corresponding to an average of the modelling period. A decrease of the planetary boundary layer height implies a reduction of the amount of turbulent mixing in the atmosphere; this reduction is directly related to the changes in the surface energy balance promoted by each "green" scenario. These results are in accordance with the findings obtained in similar studies (e.g., Fallman et al., 2016).

For a more detailed analysis, and due to the importance of air temperature and boundary layer height to the air pollutants formation, and due to the magnitude of the obtained differences, the hourly differences (by comparing the scenarios and the control run) of these variables were investigated (Fig. 2). These differences were estimated using a spatial average of the grid domain for the duration of the heat wave, to assess the averaged behaviour of the study area.

The results allowed to conclude that the majority of the analysed scenarios (S1, S2 and S3) promote an average temperature reduction throughout the study domain, with a stronger temperature decrease during the day (6 a.m.–8 p.m.). This behaviour is related to changes in the energy partitioning promoted by the implementation of the "green" measures, namely the balance between the latent and sensible heat flux; changes in the energy balance are more pronounced in the daytime

period (Rafael et al., 2016) when a higher amount of solar radiation reaches to the surface. For S4 scenario, a slight temperature increase (around $+0.1 \text{ }^\circ\text{C}$) was obtained as an average for the entire domain. This is probably related to a localised increase of temperature in the parks area due to the green area/built-up surroundings pressure gradient, which will produce a convergence of warmer air above the park (Oke et al., 1989).

Regarding the boundary layer height, all the scenarios revealed a general decrease throughout the study domain, with most pronounced differences obtained during day time in response to the diurnal cycle of heating and cooling of the surface. For S1, S2 and S3 scenarios the obtained differences are mainly related to a change of the thermal interaction between the surface and the atmosphere. It is well known that the depth and structure of the boundary layer is determined by the temperature of the updrafts and the change of temperature with height in the environment (Holtslag, 2015). As result, and since the implementation of "green" measures reduces the temperature difference between the ground surfaces (by increasing the amount of energy that is reflected) and the atmosphere, a decrease of turbulent mixing and boundary layer height is obtained. For the S4 scenario, both physical and thermal properties of the underlying surface, in conjunction with the dynamics and thermodynamics of the lower atmosphere, changes the behaviour of the boundary layer. By changing the land use (compared to control run), a change on the friction exerted by the wind against the surface elements (such as buildings and trees) was promoted; this friction causes the wind to be sheared and creates turbulence (LeMone, 2015), which defined the depth of boundary layer. An increase of the boundary layer height was observed between 12 a.m. and 8 p.m. (an increase less than $+5 \text{ m}$), which is also justified by an increase of air temperature. After sunset, particularly during early morning, when turbulence decays in the boundary layer, the effect of "green" measures can be neglected.

The variation of the boundary layer plays a critical role for dictating the dispersion of pollutants since most pollutants are emitted or formed in the boundary layer.

The spatial effects of the studied measures were also investigated. Fig. 3 shows the temperature mean differences fields for all the analysed scenarios. The results revealed that S1, S2 and S3 scenarios clearly reduce urban temperatures. Since green (S1 scenario) and white roofs (S2 scenario) were applied almost evenly across the urban area, a uniform temperature reduction was obtained throughout the study domain. In terms of effectiveness of the measures in lowering surface temperatures, the results show that the effects of evapotranspiration and increase in the surface moisture availability produced by green roofs are similar to the effects promoted by an albedo increase. S3 scenario showed a more pronounced temperature reduction, which allows to conclude that the higher the proportion of white surfaces coverage is, the higher will be the surface temperature reductions. The differences in the average temperature fields of S1 and S2 scenarios was around $-0.5 \text{ }^\circ\text{C}$, reaching $-1 \text{ }^\circ\text{C}$ in S3 scenario. Maximum differences are reached at 12 a.m., with a temperature reduction of $-5.7 \text{ }^\circ\text{C}$ for S1 scenario, and of $-5.0 \text{ }^\circ\text{C}$ for S2 and S3 scenarios.

For the S4 scenario, the mean temperature differences field showed a located pattern, with the temperature differences being located in the vicinity of the added green urban areas. The so-called park cool island effect (Spronken-Smith and Oke, 1998) is clearly visible in Fig. 3. The pressure gradient resulting from the differences of temperature between the green area (cooler) and its urbanized surroundings (warmer), leads to a cold air advection from the park to the built-up areas, known as the park cool island effect. Due to the convergence of warmer air above the park (Oke et al., 1989), a localised temperature increase was observed in the parks area. As a result, the differences in the average surface temperature fields varies between $-1 \text{ }^\circ\text{C}$ and $+1 \text{ }^\circ\text{C}$. It should also be noted that the greater the difference between the high and low pressure areas, the faster the wind will blow. In summer periods, the typical atmospheric circulation in north Atlantic coastal areas of Portugal is

southward. The interaction between the synoptic southward winds and the local scale sea breezes (which usually blows eastward), originates a south-east transport of cooler air masses from green urban areas to their surroundings. This feature is fully discussed by [Carvalho et al. \(2017\)](#).

From the point of view of minimizing the impacts of extreme events related to temperature, the application of white roofs is a viable, cost-effective and economically attractive approach.

3.2. Air quality analysis

The analysis of air quality results was made based on the spatial differences between the “green” scenarios and the control run (relative difference) for three time periods, to provide an overview of the day time effects of the studied measures. [Figs. 4–6](#) show relative hourly mean (mean over the same hour of the day for all days of the episode) differences for the near surface concentration of PM10, NO₂ and O₃.

An average increase of PM10 concentrations is obtained for S1 (+0.6%), S2 (+0.7%) and S3 (+1.5%) scenarios when compared to the control run ([Fig. 4](#)). This increase is more pronounced on the region where the urban emission sources are located (e.g., road traffic emissions). The relative changes, in terms of percentage, are not very high; however, since nowadays some exceedances to the PM10 daily limit value are observed, these changes can increase the occurrence of acute air quality problems. Maximum increases (hourly averaged for the entire episode) of PM10 concentrations can reach +38 $\mu\text{g m}^{-3}$ (+6%, S1), 52 $\mu\text{g m}^{-3}$ (+11%, S2) and 86 $\mu\text{g m}^{-3}$ (+22%, S3) in each of the analysed scenarios. PM10 daytime concentrations are higher on these scenarios, since all of them promote a reduction of near surface temperature and therefore a reduction of the vertical turbulent exchange (which can be related to the reduction of the boundary layer height). This occurs since the applied measures reduce the incoming solar radiation on the surface (and its related temperature); less heating of the surface leads to less turbulence due to the smaller heat flux ([Quan et al., 2013](#)). Similar findings for primary compounds were obtained by [Fallman et al. \(2016\)](#).

Previous studies suggested that the evolution of the PBL has a significant effect on the surface air pollutants ([Baumbach and Vogt, 2003](#); [Han et al., 2009](#); [Tie et al., 2007](#); [Velasco et al., 2008](#)). The PBL height can affect the dilution of pollutants emitted near the ground through various interactions and feedback mechanisms ([Emeis and Schäfer, 2006](#); [Su et al., 2017](#)). The PBL height can significantly impact aerosol vertical structure, as the bulk of locally generated pollutants tends to be concentrated within this layer. In fact, the study of [Quan et al. \(2013\)](#) has showed the existence of an anti-correlation between the PBL height and the PM10 concentrations. This means that as PBL height lowers, higher PM10 concentrations are obtained. The lower PBL height can in turn maintain PM10 in the PBL, leading to the increase in PM10 concentrations. This process could form a positive feedback loop, leading to continuous increase in PM10 concentration. The enhancement of PM10 concentrations tends to decrease the development of PBL by decreasing solar radiation, while the repressed structure of PBL will in turn weaken the pollutants dispersion, leading to a reduction of local air quality.

The most noteworthy differences were obtained at 12 a.m. (varying between +0.9% and +2.4% on average, for S1 and S3 scenarios, respectively) and 6 p.m. (varying between +0.4% and 2.1% on average, for S1 and S3 scenarios, respectively) due to a conjoint influence of meteorological conditions and local emissions. At these time periods the maximum reductions of temperature and incoming shortwave radiation were obtained (by comparing the scenarios and the control run), leading to the maximum reductions of PBL height. This fact, combined with a high PM10 emission rate (mostly related to the road traffic sector, which is the main emission sector at the urban area – responsible for 54% of the total emissions), led to the obtained results. It should also be noted that at the early morning, for S1 scenario, a slight and localised decrease of PM10 concentrations was obtained, due to the diurnal cycle of PBL which minimized the effect of the rapid increase of emissions.

The S4 scenario showed, on average, a decrease of PM10

concentrations, with the maximum reductions being obtained at 12 a.m. and 6 p.m. and localised in the urban area ([Fig. 4](#)). For these periods, the maximum decreases ranged between $-20 \mu\text{g m}^{-3}$ (12 a.m.) and $-17 \mu\text{g m}^{-3}$ (6 p.m.), which corresponds to a relative decrease of -45% and -36% . For the mean of the episode, maximum decreases reached -21% ($-54 \mu\text{g m}^{-3}$). This occurs due to the increase of the boundary layer height during this time, which increases the vertical turbulent exchange, promoting the dispersion of PM10. Also, the increase of natural vegetation promotes an increase of the amount of PM10 that is removed by deposition. This happens since plants have a large surface area per unit volume, increasing the probability of deposition compared with the smooth, manufactured surfaces present in urban areas ([Janhäll, 2015](#)).

As obtained for PM10, a general increase of NO₂ concentrations was found for S1, S2 and S3 scenarios ([Fig. 5](#)). The spatial distribution of these differences is similar to those obtained for PM10; however, the magnitude of the differences are unlike. For the spatial and temporal mean of the episode, an average increase of 0.8% [S1], 1.8% [S2] and 3.5% [S3] of NO₂ concentrations was obtained; maximum values can increase up to 50 $\mu\text{g m}^{-3}$ (+13% and +25.2%, for S1 and S2 scenarios) and 69 $\mu\text{g m}^{-3}$ (45%, for S3 scenario). Analysing the diurnal variation, the major differences were obtained at 12 a.m. and 6 p.m. At the later morning, average differences of +1.3% (with a maximum increment of 5 $\mu\text{g m}^{-3}$), +1.7% (with a maximum increment of 5 $\mu\text{g m}^{-3}$) and 4.3% (with a maximum increment of 11 $\mu\text{g m}^{-3}$), were obtained for S1, S2 and S3 scenarios, respectively. At the afternoon, the average increase varies between +1.4% (S1) and +7.6% (S3); maximum differences of +5.7 $\mu\text{g m}^{-3}$, 15.7 $\mu\text{g m}^{-3}$ and 20.3 $\mu\text{g m}^{-3}$ were obtained for S1, S2 and S3 scenarios. The high relative increase of daytime NO₂ can be attributed to NO, which is emitted and hampered from being diluted due to weaker atmospheric turbulence. In the course of a day NO is interconverted to NO₂, which gradually builds up during the day. NO which is emitted in the evening quickly reacts with ozone to form NO₂ again, leading to higher relative increases in NO₂ at this time.

Due to this last feature, the NO₂ and O₃ results should be analysed in an integrated way, since the change in NO₂ concentrations, due to a decrease in atmospheric mixing, can evoke a secondary impact on O₃ concentrations via chemical reactions. As discussed by [Fallmann et al. \(2016\)](#), NO₂ concentrations exhibit a negative exponential relationship with ozone; this means that, in general, the highest relative decrease of ozone is congruent with the highest levels of NO₂. The most important factor which drives this photochemical reaction in the troposphere is high energetic shortwave radiation ([Seinfeld and Pandis, 2012](#)), which means that there is a linear regression correlating ozone and temperature ([Fallmann et al., 2016](#)). This photochemical reaction boost changes in NO₂ concentrations by two main mechanisms: i) the decrease of turbulent mixing in S1, S2 and S3 scenarios, reduces the downward mixing of ozone from higher levels during this time, which inhibits the NO₂ consumption; and ii) the air temperature reduction promoted by these scenarios, inhibits the photochemical reactions and by this the ozone formation, which implies an increase of NO₂ levels near the ground.

Despite the general increase of NO₂ concentration overall the study domain, there are also small areas where decreased concentrations were found, mostly located in the surroundings of the Porto urban area. This happens due to the downwind transportation of NO₂ to areas far from its emission sources, which create conditions for O₃ formation; this formation implies a consumption of NO₂ and so a reduction of its concentration. Maximum decreases occur at 12 a.m. and 6 p.m. for the S3 scenario, with values of $-12 \mu\text{g m}^{-3}$ and $-19 \mu\text{g m}^{-3}$; for S1 and S2 scenarios the maximum decreases reach $-6.5 \mu\text{g m}^{-3}$ (at 12 a.m.) and $14.7 \mu\text{g m}^{-3}$ (at 6 p.m.).

The increase of green urban areas (S4 scenario) showed an average decrease of NO₂ concentrations around -3.4% (for the mean of the episode); maximum decreases can reach -26% , corresponding to a reduction of $-78 \mu\text{g m}^{-3}$. As previously discussed for PM10, this

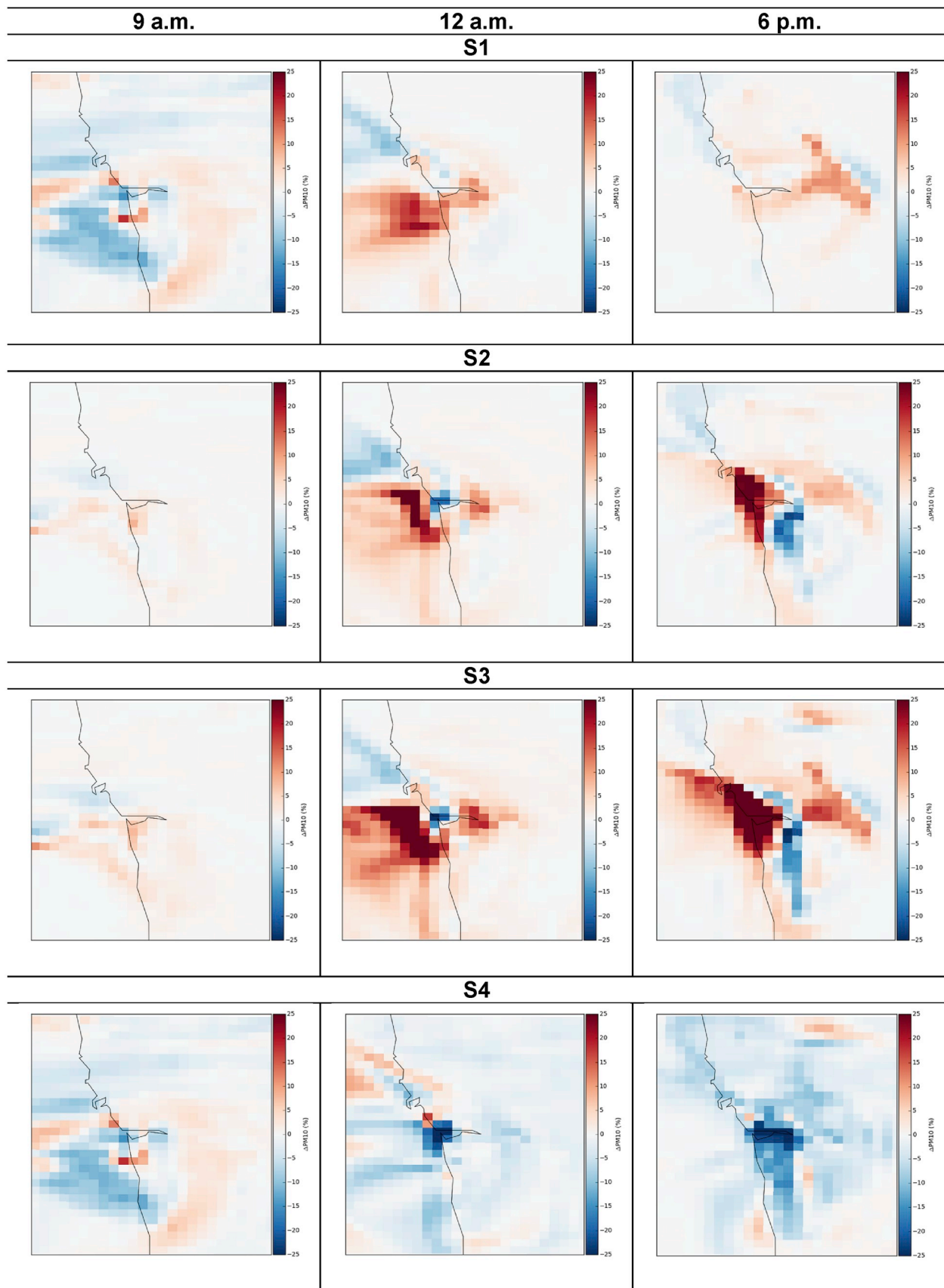


Fig. 4. Relative differences (%) between the “green” scenarios and the control run for PM10 concentrations at 9 a.m., 12 a.m. and 6 p.m. (mean over the same hour of the day for all days of the episode). (For interpretation of the references to color in this figure legend, the reader is referred to the Web version of this article.)

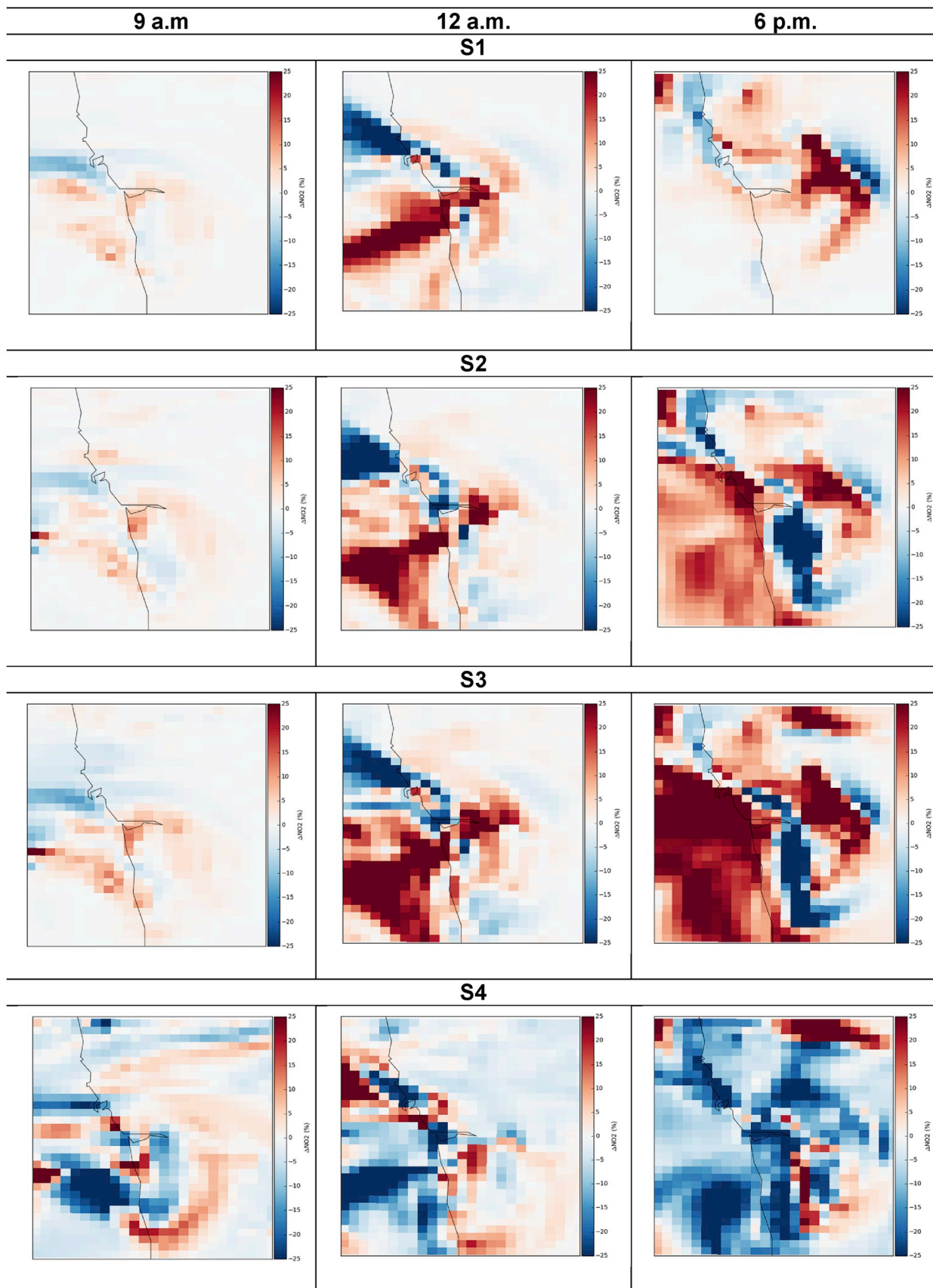


Fig. 5. Relative differences (%) between the “green” scenarios and the control run for NO₂ concentrations at 9 a.m., 12 a.m. and 6 p.m. (mean over the same hour of the day for all days of the episode). (For interpretation of the references to color in this figure legend, the reader is referred to the Web version of this article.)

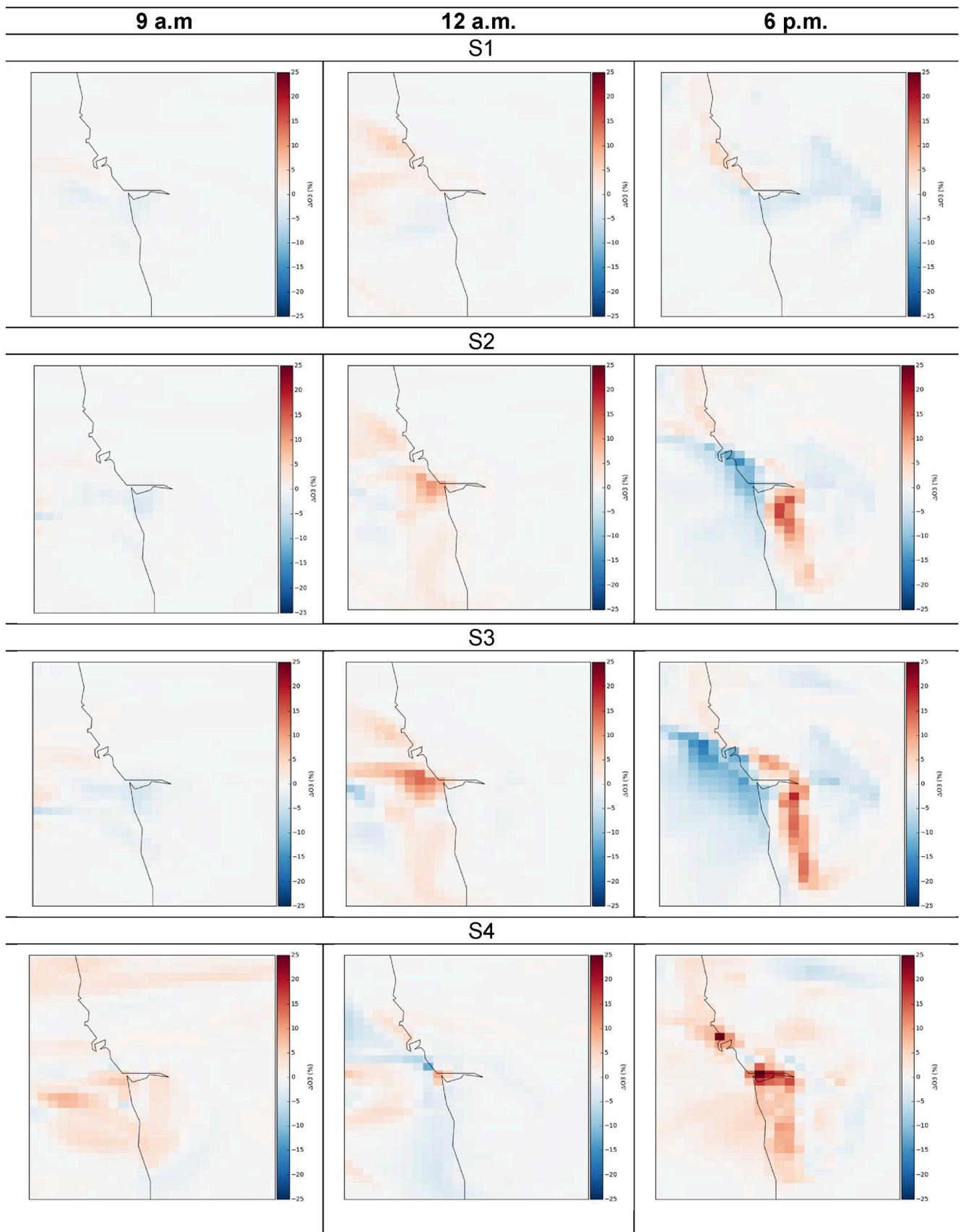


Fig. 6. Relative differences (%) between the “green” scenarios and the control run for O₃ concentrations at 9 a.m., 12 a.m. and 6 p.m. (mean over the same hour of the day for all days of the episode). (For interpretation of the references to color in this figure legend, the reader is referred to the Web version of this article.)

decrease is directly related to the increase of the boundary layer height, which promotes the vertical turbulent exchange and therefore the dispersion of NO₂. Also, due to the heterogeneity of the effects of green areas in the air temperature, an increase of the amount of NO₂ that is removed via O₃ formation is promoted in this scenario.

When analysing the effects of “green” measures on O₃ concentrations, differences lesser than 0.5% were found for the mean of the episode (Fig. 6). As concluded for PM10 and NO₂, the major differences were obtained at 12 a.m. and 6 p.m. Both positive (increase of O₃ concentrations) and negative (decrease of O₃ concentrations) differences were found, with the spatial distribution of these differences occurring in a negative correlation with the NO₂ differences. This means that areas that show an increase of NO₂ concentrations also show a decrease of O₃ concentrations; the inverse also occurs.

For S1, S2 and S3 scenarios, decreases of O₃ concentrations occur at 9 a.m. (with maximum decreases varying between -2.3% and -5.8% , representing $-2.2 \mu\text{g m}^{-3}$ and $-5.6 \mu\text{g m}^{-3}$), and increases of O₃ concentrations occur at 12 a.m. (with maximum increases varying between $+5.8\%$ and 14% , representing $6.8 \mu\text{g m}^{-3}$ and $14 \mu\text{g m}^{-3}$). Especially for the albedo scenarios (S2 and S3), at 6 p.m., a small (in terms of spatial dimensions) but a clear increase of O₃ concentrations was found. This effect can be explained by the higher reflected shortwave radiation, leading to an increase in the O₃ concentrations by up to 18.8% ($18.9 \mu\text{g m}^{-3}$). The increase in concentrations is an inadvertent effect resulting from changes in atmospheric carrying capacity (for ozone production) and in meteorology, i.e., decreased mixing height and reduced wind speed (resulting from surface-cooling effects of increased albedo). There are also small areas of decreased concentrations at this hour that can reach up to $-19.4 \mu\text{g m}^{-3}$. These reductions affect areas with largest base-case concentrations and thus are useful in offsetting the higher ozone in the domain. The main decreases occur in the surroundings of the Porto urban area, both in coastal and innermost areas of the domain, while the municipalities located south of Porto will exhibit an increment of O₃ concentrations. Similar patterns were obtained by Sá et al. (2016). According to Taha (1997) ozone concentrations for the urban area of Los Angeles and its surroundings decreased by 4.7% when increasing the surface albedo of roofs and walls from 0.2 to 0.5. A similar effect was found for the urban area of Sacramento (Taha, 2008), where the city wide albedo increase reduced ozone by about 18%.

For S4 scenario, a general increase of O₃ concentrations was found, especially located at the Porto urban area. Maximum increases occur at 6 p.m., with a value of $+30\%$ (corresponding to an increase of $+21.5 \mu\text{g m}^{-3}$). Although high levels of O₃ concentrations had been registered in some cities, it is well known that the highest values normally occur at downwind locations, since at the urban areas the ozone is rapidly consumed by local NO_x emissions (Mazzeo et al., 2005). Due to the chemical coupling of surface O₃ and NO₂, the reduction of NO₂ concentrations promoted by the implementation of green areas is accompanied by an increase in the atmospheric concentration of O₃.

Due to the role of primary Volatile Organic Compounds (VOC) in the photochemical reactions of O₃ formation, the impact of increasing vegetation on these compounds was also investigated. Very slight VOC concentration differences were obtained (around 0.1%) and thus, it can be concluded that there is no relevant correlation between simulated primary VOC (e.g. isoprene, monoterpenes, among other compounds)

and ozone concentration. This conclusion is in agreement with the results of Fallmann et al. (2016).

The obtained results highlight the importance of investigating the secondary effects of any kind of urban planning measures in the mitigation of climate change impacts, namely its impacts on the urban air quality. This is especially relevant for nature-based solutions due to their multi-functionality capability. To an easy understanding of the results, the overall impacts of the analysed measures were summarized in Table 4.

4. Conclusions

To make cities sustainable and resilient to air pollution is one of the 2030 sustainable development goals. There is a growing recognition that the implementation of options that go further than the typical technological measures is crucial to achieve this goal. Simulations with the WRF-CHIMERE modelling setup, including the single-layer urban canopy model (SLUCM), were performed for the Porto urban area for a medium-term future heat wave episode, in order to assess the capability of green measures to improve air quality. Four measures within four scenarios were analysed: i) the introduction of “cold” roofs in areas classified as built-up areas; ii) the introduction of green roofs in areas classified as built-up areas; iii) the application of “light” surfaces in areas classified as built-up area; and iv) the duplication of existing green areas.

The modelling results suggest overall benefits for all the analysed measures in the mitigation of heat waves effects, by reducing the air temperature in a range of $-0.5 \text{ }^\circ\text{C}$ and $-1 \text{ }^\circ\text{C}$ (average differences for the mean of the episode). In terms of impacts on the urban air quality, both positive and negative effects were found. For PM10 and NO₂ air pollutants, the positive effect of reduced temperature is reversed. Model results showed that a temperature reduction has a significant effect on the dynamical structure of the urban boundary layer. A decrease of turbulent kinetic energy due to a lower temperature leads to a lower rate of turbulent mixing and a decrease of the mixing layer height, thus resulting in higher near surface concentrations of these pollutants. This holds for the scenario where green roofs were implemented (S1 scenario) and for the scenarios where the albedo of building roofs and walls was increased (S2 and S3 scenarios). A maximum relative increase by 6% [S1], 11% [S2] and 22% [S3] for PM10 was found; for NO₂, maximum increases reach 13% [S1], 25% [S2] and 44% [S3]. The increase of green urban areas (S4 scenario) endorsed an increase of the mixing layer height and a higher rate of turbulent mixing, and thus, a reduction of both PM10 and NO₂ concentrations was obtained. Maximum decreases (for the mean of the episode) of -21% [PM10] and -27% [NO₂] were found.

For ozone, both positive and negative effects were found, with the spatial distribution of these differences occurring in a negative correlation with the NO₂ differences. For S1, S2 and S3 scenarios, decreases of O₃ concentrations occur at 9 a.m. and increases of O₃ concentrations occurs at 12 a.m. Beyond the linkages between the NO₂ and O₃ concentrations, the increase of O₃ levels in these scenarios was explained by the higher reflected shortwave radiation, which accelerates photochemical reactions triggers ozone formation. For S4 scenario, an increase of O₃ concentrations was found, mainly over the Porto urban area. Maximum increases occur at 6 p.m., with a value of $+30\%$.

Table 4

Summary of the overall impacts of “green” measures on both meteorological (temperature) and air quality (PM10, NO₂ and O₃) parameters. The ↓ denotes a decrease and ↑ symbolises an increase.

	“Green” measures			
	Implementation of green roofs (S1)	Implementation of white roofs (S2)	Implementation of white surfaces (S3)	Implementation of parks (S4)
T	↓	↓	↓	↓↑
PM10	↑	↑	↑	↓
NO ₂	↑	↑	↑	↓
O ₃	↓↑	↓↑	↓↑	↑

This type of results show that changes in urban planning can influence both climate and air quality of urban areas. The main advantage of this approach is the study of a set of measures (through a quantification of its effectiveness) in a short period of time. Also, the approach can be applied to other cities. This is highly advantageous for policy makers and stakeholders' decision making. Despite of that, it was not the purpose of this paper to develop a recommendation for the implementation of a particular measure, as different positive and negative effects have to be traded off against each other and more detailed studies will be required for such a decision. This work provides a modelling case study for a medium size European city with a high rate of population density. For cities with different morphologies, location, emission or meteorological conditions the same measures might have different effects on air quality.

Also, certain issues and caveats need to be addressed with further detail in the future. This case study deals only with the assessment of the effects of "green" measures on air quality based on changes in the meteorological conditions, and so do not consider changes in emissions. Additional studies should be carried out to consider the effect of changes in the meteorological conditions along with changing emissions. Furthermore, the effects of the studied measures under other meteorological conditions, investigating, for example, the seasonal behaviour, should be analysed.

Declaration of competing interest

The authors declare that they have no known competing financial interests or personal relationships that could have appeared to influence the work reported in this paper.

CRediT authorship contribution statement

S. Rafael: Writing - original draft, Conceptualization, Methodology. **B. Augusto:** Software. **A. Ascenso:** Software. **C. Borrego:** Writing - review & editing. **A.I. Miranda:** Writing - review & editing.

Acknowledgements

This work was supported by the project FUTURAR (PTDC/AAG-MAA/2569/2014-POCI-01-0145-FEDER-016752) funded by FEDER, through COMPETE2020 - Programa Operacional Competitividade e Internacionalização (POCI), and by national funds, through FCT/MCTES; by UNaLab project that has received funding from the European Union Horizon 2020 research and innovation programme under Grant Agreement No. 730052, Topic: SCC-2-2016-2017: Smart Cities and Communities Nature based solutions; and by the project GENESIS (PTDC/GES-URB/29444/2017) funded by FCT/MCTES through national funds and by the European Community Fund FEDER within the COMPETE2020 program.

Thanks are also due for the financial support to the PhD grant of A. Ascenso (SFRH/BD/136875/2018), and to CESAM (UID/AMB/50017/2019), to FCT/MCTES through national funds, and the co-funding by the FEDER, within the PT2020 Partnership Amorim et al., 2013.

Appendix A. Supplementary data

Supplementary data to this article can be found online at <https://doi.org/10.1016/j.atmosenv.2019.117123>.

References

- European Environment Agency - EEA, 2011. The Application of Models under the European Union's Air Quality Directive: A Technical Reference Guide. Publications Office of 579 the European Union, Luxembourg, ISBN 978-92-9213-223-1.
- Environmental European Agency - EEA, 2016. Urban Adaptation to Climate Change in Europe 2016 - Transforming Cities in a Changing Climate. EEA Report No 12/2016. Publications Office of the European Union, Luxembourg, ISBN 978-92-9213-742-7, 2016.
- Environmental European Agency - EEA, 2017. Air Quality in Europe — 2017 Report. EEA Report No 13/2017. Publications Office of the European Union, Luxembourg, ISBN 978-92-9213-921-6, 2017.
- Amorim, J.H., Rodrigues, V., Tavares, R., Valente, J., Borrego, C., 2013. CFD modelling of the aerodynamic effect of trees on urban air pollution dispersion. *Sci. Total Environ.* 461–462, 541–551.
- Baumbach, G., Vogt, U., 2003. Influence of inversion layers on the distribution of air pollutants in urban areas. *Water Air Soil Pollut.* 3, 65–76.
- Bessagnet, B., Hodzic, A., Vautard, R., Beekmann, M., Cheinet, S., Honoré, C., Rouil, L., 2004. Aerosol modelling with CHIMERE—preliminary evaluation at the continental scale. *Atmos. Environ.* 38, 2803–2817.
- Borrego, C., Monteiro, A., Martins, H., Ferreira, J., Fernandes, A.P., Rafael, S., Miranda, A.I., Guevara, M., Baldasano, J.M., 2015. Air quality plan for ozone: an urgent need for North Portugal. *Air Qual Atmos Health* 9, 447–460. <https://doi.org/10.1007/s11869-015-0352-5>.
- Brands, S., Herrera, S., Fernández, J., Gutiérrez, J.M., 2013. How well do CMIP5 Earth System Models simulate present climate conditions in Europe and Africa? *Clim. Dyn.* 41, 803–817.
- Büttner, G., Feranec, G., Jaffrain, G., 2006. Corine land cover nomenclature illustrated guide (Addendum 2006). <http://eea.eionet.europa.eu/Members/irc/eionetcircle/spatial/library/?l=/clc2005update/clc2006technical/draft/nomenclaturedoc/E%20N1.0&a=d>.
- Carvalho, M.J., Melo-Gonçalves, P., Rocha, A., 2014. CMIP5 – performance and climate change assessment of maximum and minimum temperatures in Europe. EMS annual meeting abstracts. In: 14th EMS Annual Meeting & 10th European Conference on Applied Climatology (ECAC), vol. 11, p. EMS2014.
- Carvalho, D., Martins, H., Marta-Almeida, M., Rocha, A., Borrego, C., 2017. Urban resilience to future urban heat waves under a climate change scenario: a case study for Porto urban area (Portugal). *Urban Clim.* 19, 1–27.
- Chen, F., Kusaka, H., Bornstein, R., Ching, J., Grimmond, C.S.B., Grossman-Clarke, S., Loridan, T., Manning, K.W., Martilli, A., Miao, S., Sailor, D., Salamanca, F.P., Taha, H., Tewari, M., Wang, X., Wyszogrodzki, A.A., Zhang, C., 2011. The integrated WRF/urban modelling system: development, evaluation, and applications to urban environmental problems. *Int. J. Climatol.* 31, 273–288.
- Chen, L., Zhang, M., Zhu, J., Wang, Y., Skorokhod, A., 2018. Modelling impacts of urbanization and urban heat island mitigation on boundary layer meteorology and air quality in Beijing under different weather conditions. *J. Geophys. Res.: Atmos.* 123, 4323–4344. <https://doi.org/10.1002/2017JD027501> [doi: 10.1002/2017JD027501].
- Dudhia, J., 1989. Numerical study of convection observed during the winter monsoon experiment using a mesoscale two-dimensional model. *J. Atmos. Sci.* 46, 3077–3107.
- Emeis, S., Schäfer, K., 2006. Remote sensing methods to investigate boundary-layer structures relevant to air pollution in cities. *Boundary-Layer Meteorol.* 121, 377–385, 2006.
- Epstein, S.A., Lee, S.-M., Katzenstein, A.S., Carreras-Sospedra, M., Zhang, X., Farina, S.C., Vahmani, P., Fine, P.M., BanWeiss, G., 2017. Air-quality implications of widespread adoption of cool roofs on ozone and particulate matter in southern California. In: Proceedings of the National Academy of Sciences (PNAS), vol. 114, pp. 8991–8996. <https://doi.org/10.1073/pnas.1703560114>.
- European Commission - EC, 2015. Towards an EU Research and Innovation Policy Agenda for Nature-Based Solutions & Re-naturing Cities. Final Report of the Horizon 2020 Expert Group on 'Nature-Based Solutions and Re-naturing Cities'. Publications Office of the European Union, Luxembourg, ISBN 978-92-79-46051-7.
- Fallmann, J., Forkel, R., Emeis, S., 2016. Secondary effects of urban heat island mitigation measures on air quality. *Atmos. Environ.* 125, 199–211. <https://doi.org/10.1016/j.atmosenv.2015.10.094>.
- Fallmann, J., Emeis, S., Suppan, P., 2013. Mitigation of urban heat stress – a modelling case study for the area of Stuttgart. *DIE ERDE - J. Geogr. Soc. Berl.* 144, 202–216. <https://doi.org/10.12854/erde-144-15>.
- Fonseca, D., Carvalho, M.J., Marta-Almeida, M., Melo-Gonçalves, P., Rocha, A., 2016. Recent trends of extreme temperature indices for the Iberian Peninsula. *Phys. Chem. Earth.* <https://doi.org/10.1016/j.pce.2015.12.005>.
- Gama, C., Monteiro, A., Pio, C., Miranda, A.I., Baldasano, J., Tchepel, O., 2018. Temporal patterns and trends of particulate matter over Portugal: a long-term analysis of background concentrations. *Air Qual Atmos. Health* 11, 397–407. <https://doi.org/10.1007/s11869-018-0546-8>.
- Giorgetta, M.A., Jungclaus, J., Reick, C.H., Legutke, S., Bader, J., Böttinger, M., Brovkin, V., Crueger, T., Esch, M., Fieg, K., Glushak, K., Gayler, V., Haak, H., Hollweg, H.-D., Ilyina, T., Kinne, S., Kornbluh, L., Matei, D., Mauritsen, T., Mikolajewicz, U., Mueller, W., Notz, D., Pithan, F., Raddatz, T., Rast, S., Redler, R., Roeckner, E., Schmidt, H., Schnur, R., Segsneider, J., Six, K.D., Stockhause, M., Timmreck, C., Wegner, J., Widmann, H., Wieners, K.-H., Claussen, M., Marotzke, J., Stevens, B., 2013. Climate and carbon cycle changes from 1850 to 2100 in MPI-ESM simulations for the Coupled Model Intercomparison Project phase 5. *J. Adv. Model. Earth Syst.* 5, 572–597.
- Grell, G.A., 1993. Prognostic evaluation of assumptions used by cumulus parameterization. *Mon. Weather Rev.* 121, 764–787.
- Grell, G.A., Devenyi, D., 2002. A generalized approach to parameterizing convection combining ensemble and data assimilation techniques. *Geophys. Res. Lett.* 29, 1693. <https://doi.org/10.1029/2002GL015311>.
- Guenther, A., Karl, T., Harley, P., Wiedinmyer, C., Palmer, P.I., Geron, C., 2006. Estimates of global terrestrial isoprene emissions using MEGAN (model of emissions of gases and aerosols from nature). *Atmos. Chem. Phys.* 6, 3181–3210.
- Han, S.Q., Bian, H., Tie, X., Xie, Y., Sun, M., Liu, A., 2009. Impact measurements of nocturnal planetary boundary layer on urban air pollutants: from a 250-m tower over Tianjin, China. *J. Hazard Mater.* 162, 264–269.

- Hauglustaine, D.A., Hourdin, F., Jourdain, L., Filiberti, M.-A., Walters, S., Lamarque, J.-F., Holland, E.A., 2004. Interactive chemistry in the Laboratoire de Météorologie Dynamique general circulation model: description and background tropospheric chemistry evaluation. *J. Geophys. Res.: Atmos.* 109.
- Holtslag, A., 2015. Boundary layer (atmospheric) and air pollution - modeling and parameterization. Reference module in earth systems and environmental sciences. *Encyclopaedia. Atmos. Sciences* 265–273. <https://doi.org/10.1016/B978-0-12-382225-3.00087-6>.
- Hong, S.-Y., Lim, J.-O.-J., 2006. The WRF single-moment 6-class microphysics scheme (WSM6). *Asia Pac. J. Atmos. Sci.* 42, 129–151.
- Hong, S.-Y., Noh, Y., Dudhia, J., 2006. A new vertical diffusion package with an explicit treatment of entrainment processes. *Mon. Weather Rev.* 134, 2318–2341.
- INE (Instituto Nacional de Estatística) – Statistics Portugal, 2011. CENSUS, 2011 - Statistical Data for Portugal [Internet]. Available from: <http://censos.ine.pt>.
- Intergovernmental Panel on Climate Change – IPCC, 2013. Summary for policymakers. In: Stocker, T.F., Qin, D., Plattner, G.-K., Tignor, M., Allen, S.K., Boschung, J., Nauels, A., Xia, Y., Bex, V., Midgley, P.M. (Eds.), *Climate Change 2013: the Physical Science Basis. Contribution of Working Group I to the Fifth Assessment Report of the Intergovernmental Panel on Climate Change*. Cambridge University Press, Cambridge, United Kingdom and New York, NY, USA.
- Janhäll, S., 2015. Review on urban vegetation and particle air pollution – deposition and dispersion. *Atmos. Environ.* 105, 130–137. <https://doi.org/10.1016/j.atmosenv.2015.01.052>.
- Kusaka, H., Kimura, F., 2004. Thermal effects of urban canyon structure on the nocturnal heat island: numerical experiment using a mesoscale model coupled with an urban canopy model. *J. Appl. Meteorol.* 43, 1899–1910.
- Kusaka, H., Kondo, H., Kikigawa, Y., Kimura, F., 2001. A simple single layer urban canopy model for atmospheric models: comparison with multi-layer and slab models. *Boundary-Layer Meteorol.* 101, 329–358.
- Lau, K.K., Lindberg, F., Rayner, D., Thorsson, S., 2015. The effect of urban geometry on mean radiant temperature under future climate change: a study of three European cities. *Int. J. Biometeorol.* 59, 799–814.
- LeMone, B., 2015. Boundary layer (atmospheric) and air pollution - convective Boundary Layer. Reference Module in Earth Systems and Environmental Sciences. *Encyclopaedia of Atmospheric Sciences*, pp. 250–257. <https://doi.org/10.1016/B978-0-12-382225-3.00085-2>.
- Li, D., Bou-Zeid, E., Barlage, M., Chen, F., Smith, J.A., 2013. Development and evaluation of a mosaic approach in the WRF-Noah framework. *J. Geophys. Res.: Atmos.* 118, 1–18.
- Manders, A.M.M., van Meijgaard, E., Mues, A.C., Kranenburg, R., van Ulfst, L.H., Schaap, M., 2012. The impact of differences in large-scale circulation output from climate models on the regional modeling of ozone and PM. *Atmos. Chem. Phys.* 12, 9441–9458.
- Markakis, K., Valari, M., Colette, A., Sanchez, O., Perrussel, O., Honore, C., Vautard, R., Kilmont, Z., Rao, S., 2014. Air quality in the mid-21st century for the city of Paris under two climate scenarios; from the regional to local scale. *Atmos. Chem. Phys.* 14, 7323–7340.
- Marta-Almeida, M., Teixeira, J., Carvalho, M., Melo-Gonçalves, P., Rocha, A., 2016. High resolution climatic simulations for the Iberian Peninsula: model validation. *Phys. Chem. Earth* 94, 94–105. <https://doi.org/10.1016/j.pce.2016.03.010>.
- Mazzeo, N., Venegas, L., Choren, H., 2005. Analysis of NO, NO₂, O₃ and NOx concentrations measured at a green area of Buenos Aires City during wintertime. *Atmos. Environ.* 39, 3055–3068. <https://doi.org/10.1016/j.atmosenv.2005.01.029>.
- Mlawer, E.J., Taubman, S.J., Brown, P.D., Iacono, M.J., Clough, S.A., 1997. Radiative transfer for inhomogeneous atmospheres: RRTM, a validated correlated-k model for the longwave. *J. Geophys. Res.* 102D, 16663–16682.
- Monteiro, A., Velho, S., 2014. Health heat stress in the Porto metropolitan area – a matter of temperature or inadequate adaptation? *J. Geogr. Soc. Berl.* 145.
- Monteiro, A., Vautard, R., Borrego, C., Miranda, A.I., 2005. Long-term simulations of photo oxidant pollution over Portugal using the CHIMERE model. *Atmos. Environ.* 39, 3089–3101.
- Oke, T.R., Crowther, J.M., McNaughton, K.G., Monteith, J.L., Gardiner, B., 1989. The micrometeorology of the urban forest [and discussion]. *Philos. Trans. R. Soc. Biol. Sci.* 324, 335–349.
- Pineda, N., Jorba, O., Jorge, J., Baldasano, J.M., 2004. Using NOAA AVHRR and SPOT VGT data to estimate surface parameters: application to a mesoscale meteorological model. *Int. J. Remote Sens.* 25, 129–143.
- Quan, J., Gao, Y., Zhang, Q., Tie, X., Cao, J., Han, S., Meng, J., Chen, P., Zhao, D., 2013. Evolution of planetary boundary layer under different weather conditions, and its impact on aerosol concentrations. *Particuology* 11, 34–40. <https://doi.org/10.1016/j.partic.2012.04.005>.
- Rafael, S., Martins, H., Sa, E., Carvalho, D., Borrego, C., Lopes, M., 2016. Influence of urban resilience measures in the magnitude and behaviour of energy fluxes in the city of Porto (Portugal) under a climate change scenario. *Sci. Total Environ.* 566, 1500–1510. <https://doi.org/10.1016/j.scitotenv.2016.06.037>.
- Rafael, S., Martins, H., Marta-Almeida, M., Sa, E., Coelho, S., Rocha, A., Borrego, C., Lopes, M., 2017. Quantification and mapping of urban fluxes under climate change: application of WRF-SUEWS model to Greater Porto area (Portugal). *Environ. Res.* 155, 321–334. <https://doi.org/10.1016/j.envres.2017.02.033>.
- Rafael, S., Vicente, B., Rodrigues, V., Miranda, A.I., Borrego, C., Lopes, M., 2018. Impacts of green infrastructures on aerodynamic flow and air quality in Porto's urban area. *Atmos. Environ.* 190, 317–330. <https://doi.org/10.1016/j.atmosenv.2018.07.044>.
- Rafael, S., Rodrigues, V., Fernandes, A.P., Augusto, B., Borrego, C., Lopes, M., 2019. Evaluation of urban surface parameterizations in WRF model using energy fluxes measurements in Portugal. *Urban Clim.* 28, 100465. <https://doi.org/10.1016/j.uclim.2019.100465>.
- Riahi, K., Gruebler, A., Nakicenovic, N., 2007. Scenarios of long-term socio-economic and environmental development under climate stabilization. *Technol. Forecast. Soc. Chang.* 74, 887–935.
- Russo, S., Dosio, A., Graversen, R.G., Sillmann, J., Carrao, H., Dunbar, M.B., Singleton, A., Montagna, P., Barbola, P., Vogt, J.V., 2014. Magnitude of extreme heat waves in present climate and their projection in a warming world. *J. Geophys. Res.: Atmos.* 119, 500–512.
- Sá, E., Martins, H., Ferreira, J., Marta-Almeida, M., Rocha, A., Carvalho, A., Freitas, S., Borrego, C., 2016. Climate change and pollutant emissions impacts on air quality in 2050 over Portugal. *Atmos. Environ.* 131, 209–224. <https://doi.org/10.1016/j.atmosenv.2016.01.040>.
- Schmidt, H., Derognat, C., Vautard, R., Beekmann, M., 2001. A comparison of simulated and observed ozone mixing ratios for the summer of 1998 in Western Europe. *Atmos. Environ.* 35, 6277–6297.
- Seinfeld, J., Pandis, S., 2012. *Atmospheric Chemistry and Physics: from Air Pollution to Climate Change*. John Wiley & Sons, 2012.
- Skamarock, W.C., Klemp, J.B., Dudhia, J., Gill, D.O., Barker, D.M., Huang, X.Y., Wang, W., Powers, J.G., 2008. A Description of the Advanced Research WRF Version 3. NCAR/TN-475+STR, p. 113.
- Spronken-Smith, R.A., Oke, T.R., 1998. The thermal regime of urban parks in two cities with different summer climates. *Int. J. Remote Sens.* 19, 2085–2104.
- Su, T., Li, J., Li, C., Lau, A.K.H., Yang, D., Shen C., 2017. An intercomparison of AOD-converted PM_{2.5} concentrations using different approaches for estimating aerosol vertical distribution. *Atmos. Environ.* 166, 531–542.
- Susca, T., 2012. Enhancement of life cycle assessment (LCA) methodology to include the effect of surface albedo on climate change: comparing black and white roofs. *Environ. Pollut.* 163, 48–54.
- Taha, H., 1997. Modelling the impacts of large-scale albedo changes on ozone air quality in the South Coast air Basin. *Atmos. Environ.* 31, 1667–1676. [https://doi.org/10.1016/S1352-2310\(96\)00336-6](https://doi.org/10.1016/S1352-2310(96)00336-6) [doi].
- Taha, H., 2008. Meso-urban meteorological and photochemical modeling of heat island mitigation. *Atmos. Environ.* 42, 8795–8809. <https://doi.org/10.1016/j.atmosenv.2008.06.036>.
- Tie, X., Madronich, S., Li, G.H., Ying, Z.M., Zhang, R., Garcia, A., Lee-Taylor, J., Liu, Y., 2007. Characterizations of chemical oxidants in Mexico City: a regional chemical/dynamical model (WRF-Chem) study. *Atmos. Environ.* 41, 1989–2008.
- Tiwari, A., Kumar, P., Baldauf, R., Zhang, K., Pilla, F., Sabatino, S., Brattich, E., Pulvirenti, B., 2019. Considerations for evaluating green infrastructure impacts in microscale and macroscale air pollution dispersion models. *Sci. Total Environ.* 672, 410–426. <https://doi.org/10.1016/j.scitotenv.2019.03.350>.
- Vautard, R., Honoré, C., Beekmann, M., Rouil, L., 2005. Simulation of ozone during the August 2003 heat wave and emission control scenarios. *Atmos. Environ.* 39, 2957–2967.
- Velasco, E., Márquez, C., Bueno, E., Bernabé, R.M., Sánchez, A., Fentanes, O., Wöhrenschiemmel, H., Cardenas, B., Kamilla, A., Wakamatsu, S., Molina, L.T., 2008. Vertical distribution of ozone and VOCs in the low boundary layer of Mexico City. *Atmos. Chem. Phys.* 8, 3061–3079. <http://www.atmos-chem-phys.net/8/3061/2008/>.
- Vestrev, V., Adams, M., Goodwin, J., 2004. Inventory Review 2004 - Emission Data Reported to CLRTAP and under the NEC Directive. - Initial Review for HMs and POPs. EMEP Status Report. Norwegian Meteorological Institute, Oslo, p. 14.
- Vicente, B., Rafael, S., Rodrigues, V., Relvas, H., Vilaça, M., Teixeira, J., Bandeira, J., Coelho, M., Borrego, C., 2018. Influence of different complexity levels of road traffic models on air quality modelling at street scale. *Air Qual Atmos. Health* 11, 1217–1232. <https://doi.org/10.1007/s11869-018-0621-1>.
- Yang, J., Wang, Z.-H., Chen, F., Miao, S., Tewari, M., Voogt, J.A., Myint, S., 2015. Enhancing hydrologic modelling in the coupled weather research and forecasting - urban modelling system. *Boundary-Layer Meteorol.* 155, 87–109.
- Zhang, Y., Liu, X.-H., Olsen, K., Wang, W.-X., Do, B., Bridgers, G., 2010. Responses of future air quality to emission controls over North Carolina, part II: analyses of future-year predictions and their policy implications. *Atmos. Environ.* 44, 2767–2779.